



UNIVERSITY OF LEEDS

This is a repository copy of *High-Power Gallium Nitride HIFU Transmitter with Integrated Real-Time Current and Voltage Measurement*.

White Rose Research Online URL for this paper:  
<http://eprints.whiterose.ac.uk/172490/>

Version: Accepted Version

---

**Article:**

Carpenter, T [orcid.org/0000-0001-5676-1739](https://orcid.org/0000-0001-5676-1739), Cowell, D, Clegg, H et al. (2 more authors) (2021) High-Power Gallium Nitride HIFU Transmitter with Integrated Real-Time Current and Voltage Measurement. IEEE Transactions on Biomedical Circuits and Systems. ISSN 1932-4545

<https://doi.org/10.1109/tbcas.2021.3067842>

---

© 2021 IEEE. Personal use of this material is permitted. Permission from IEEE must be obtained for all other uses, in any current or future media, including reprinting/republishing this material for advertising or promotional purposes, creating new collective works, for resale or redistribution to servers or lists, or reuse of any copyrighted component of this work in other works. Uploaded in accordance with the publisher's self-archiving policy.

**Reuse**

Items deposited in White Rose Research Online are protected by copyright, with all rights reserved unless indicated otherwise. They may be downloaded and/or printed for private study, or other acts as permitted by national copyright laws. The publisher or other rights holders may allow further reproduction and re-use of the full text version. This is indicated by the licence information on the White Rose Research Online record for the item.

**Takedown**

If you consider content in White Rose Research Online to be in breach of UK law, please notify us by emailing [eprints@whiterose.ac.uk](mailto:eprints@whiterose.ac.uk) including the URL of the record and the reason for the withdrawal request.



[eprints@whiterose.ac.uk](mailto:eprints@whiterose.ac.uk)  
<https://eprints.whiterose.ac.uk/>

# High-Power Gallium Nitride HIFU Transmitter with Integrated Real-Time Current and Voltage Measurement

Thomas M. Carpenter<sup>†</sup>, David M. J. Cowell, Harry R. Clegg, James R. McLaughlan, Steven Freear

**Abstract**—High-Intensity Focused Ultrasound (HIFU) therapy provides a non-invasive technique with which to destroy cancerous tissue without using ionizing radiation. To drive large single-element HIFU transducers, ultrasound transmitters capable of delivering high powers at relevant frequencies are required. The acoustic power delivered to a transducers focal region will determine the treated area, and due to safety concerns and intervening layers of attenuation, control of this output power is critical.

A typical setup involves large inefficient linear power amplifiers to drive the transducer. Switched mode transmitters allow for a more compact drive system with higher efficiencies, with multi-level transmitters allowing control over the output power. Real-time monitoring of power delivered can avoid damage to the transducer and injury to patients due to over treatment, and allow for precise control over the output power.

This study demonstrates a transformer-less, high power, switched mode transmit transmitter based on Gallium-Nitride (GaN) transistors that is capable of delivering peak powers up to 1.8 kW at up to 600 Vpp, while operating at frequencies from DC to 5 MHz. The design includes a 12 bit 16 MHz floating Current/Voltage (I-V) measurement circuit to allow real-time high-side monitoring of the power delivered to the transducer allowing use with multi-element transducers.

**Index Terms**—HIFU, Power Amplifiers, Gallium Nitride Transistors

## I. INTRODUCTION

WHEN used in therapy applications, High-Intensity Focused Ultrasound (HIFU) provides a non-invasive technique with which to damage tissues and cause thermal lesioning without using ionizing radiation. This is achieved both through temperature rises in the tissues from acoustic absorption [1], [2], and through mechanical effects such as cavitation [3]–[5]. HIFU techniques make use of ultrasound transducers that require large electrical powers (>10 W) for sustained periods, in the order of seconds, to generate the necessary acoustic pressures *in situ*.

In a typical large element HIFU system, a linear power amplifier in conjunction with a signal generator will be used to drive the transducer. Such systems provide the necessary amplitude and phase control whilst minimizing harmonic

distortion. However, such systems are expensive, physically large [6], and suffer from poor electrical efficiency. This is especially problematic when moving towards multiple large element transducers [7] to facilitate techniques such as beam steering and dynamic focus.

The volume of the treated region is related to the total acoustic power being delivered by the transducer, the size of the focal region, and the positioning of the focal point of the transducer (i.e. attenuation layers, blood perfusion). It is therefore important to be able to control the amount of power delivered, and to monitor the output to ensure the power levels are accurate and safe. Inaccurate power delivery can have detrimental impacts on not only the system, through transducer damage from overpower conditions [8], but also to the patient. Underexposure through power levels being too low, whilst not damaging, may cause failed treatments due to insufficient heating. Overexposure, caused by excessive power delivery, can be highly dangerous to patient safety by causing significant heating and damage to surrounding tissues in the patient.

In this paper a high-power Gallium-Nitride (GaN) transistor based transmitter for HIFU applications is presented. The structure of the transmitter uses a push-pull 5-level design with low impedance output drive capabilities. The transmitter additionally contains with a fully integrated high-side power-monitoring circuit, to allow real-time measurement of the output current and voltage of the transmitter to allow accurate control over the power delivered.

## II. SWITCHED MODE TRANSMITTERS

Switched-mode amplifiers offer an alternative which can provide reduced size, lower cost, and higher efficiency than linear amplifiers [9]–[11]. Such circuits range from bi-level circuits, to multi-level circuits capable of creating stepped waveforms. As a consequence of the limited number of levels however, the waveforms generated by such circuits introduce unwanted harmonics, delivering large powers at the third and fifth harmonic in particular [12]. As typical HIFU transducers are particularly resonant at these harmonics [13], [14], this energy can be converted into acoustic power, reducing their efficacy and compromising depth penetration.

In order to achieve harmonic control, bi-level circuits such as the Class D and DE designs shown in Figure 1a [10], [15], typically use passive output filters which must be capable of handling high continuous output powers and must be

This work was supported in part by the Engineering and Physical Research Council (EPSRC) under grant number EP/S001069/1.

Authors are with the Ultrasonics and Instrumentation Group, School of Electronic and Electrical Engineering, Faculty of Engineering and Physical Sciences, University of Leeds, Leeds, LS2 9JT, UK (e-mail: <sup>†</sup>t.carpenter@leeds.ac.uk)

J. R. McLaughlan is with Leeds Institute of Medical Research, St James' University Hospital, Leeds, LS9 7TF, UK

matched to the transducer. Multi-level switched circuits on the other hand use a stepped waveform with a series of discrete voltage levels to approximate an analogue waveform, with harmonic output reduced using waveform design techniques such as Harmonic-Reduction Pulse-Width Modulation (HRPWM) [16]–[18].

HRPWM has been previously shown to allow amplitude control, whilst simultaneously providing partial cancellation of the third and fifth harmonics. Typically, the 3rd harmonic is targeted for reduction to avoid strong transducer resonances. The waveforms are additionally designed symmetrically across positive and negative rails, which when combined with time symmetry ensures no even harmonics in the waveform design. The waveforms still ultimately have many high order harmonics extending to theoretically infinite bandwidth, however the limited bandwidth of ultrasound transducers means these high order harmonics have little to no impact on the acoustic output of the transducer.

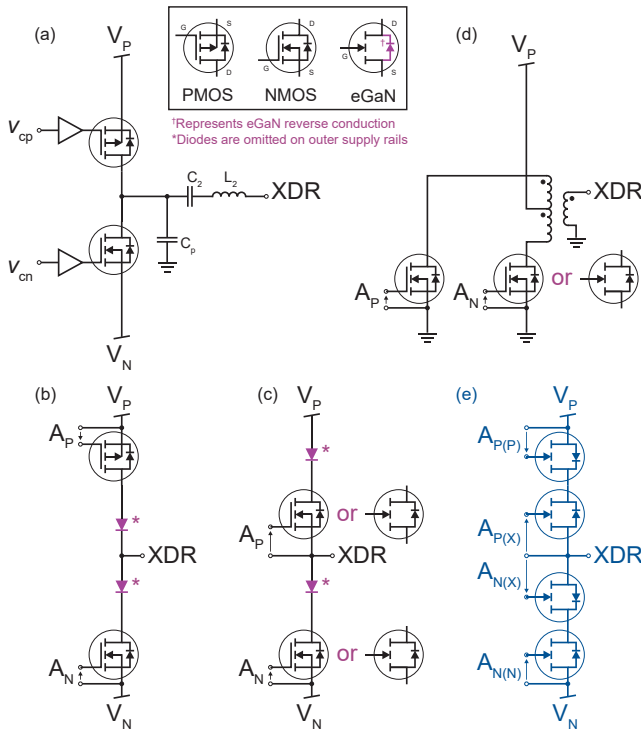


Fig. 1. Ultrasound transmitter architectures. (a) A class DE power amplifier [10]. (b) A typical PMOS/NMOS half-bridge topology [19]. (c) An alternate half-bridge topology using all NMOS with floating gate drive [20]. (d) An all NMOS two-level push-pull transmitter using centre tapped transformer. (e) Proposed push-pull transformer-less topology using all-NMOS GaN FETs.

A typical switched topology for multi-level waveforms makes use of a series of PMOS/NMOS bridges, with series diodes to prevent reverse conduction through the Metal-Oxide-Semiconductor Field Effect Transistor (MOSFET) body diode, as shown in Figure 1b. These diodes place speed restrictions on the transmitters due to reverse recovery times, whilst also dissipating large amounts of power due to their forward voltage drop. To generate HRPWM waveforms, a high switching speed is required due to the stepped nature of the waveforms. The diodes have a major impact on the generation of these

waveforms, as they remove the ability of the transmitter to pull inwards from the outer rails to the mid rails, resulting in slow inward transitions which cause a large second harmonic distortion [21]. For large HIFU transducers, high drive voltages are required to generate sufficient output power, which further pushes the thermal limitations of silicon power MOSFETs.

It is possible to increase the performance of switched transmitters by eliminating the PMOS transistors, opting for an all NMOS topology, as charge carrier mobility in NMOS transistors is higher than that of PMOS transistors, allowing for faster switching and lower losses. However, PMOS and NMOS transistors are not directly interchangeable, so alternative circuit topologies need to be considered. Switching to an all-N topology provides the added benefit of allowing the use of higher performance transistor technology such as Silicon-Carbide (SiC) or GaN devices.

Half-bridge designs using all-NMOS transistors, such as shown in Figure 1c, are common in power converter applications, however these typically either switch at much lower frequencies allowing for simplified gate-drive, or are limited to unipolar operation due to the bootstrapping circuits used to drive the high-side NMOS transistors that replace the PMOS transistors in complementary half-bridges. The use of an isolated DC-DC power supply is presented [20] instead of using bootstrap circuits for their unipolar transmitter design. The use of isolated DC-DC supplies can allow for development of bipolar bridges by providing a floating power source for digital gate isolation technologies.

One possible topology change is to use centre-tapped transformers as this allows all transistors to be referenced to ground for easier control, as shown in Figure 1d. [22]–[24] demonstrate the use of a transformer to produce an entirely NMOS bipolar transmitter. [23] additionally makes use of GaN devices for better power handling capabilities. However, the power handling of miniature transformers is limited which is problematic for Continuous Wave (CW) applications, and the use of transformers limits the bandwidth of the transmitter. Multiple transformer windings would be required to extend such a transmitter design to the multi-level designs ( $\geq 3$ -Level) required for harmonic reduction techniques and amplitude control techniques, placing further burden on the transformer design.

The diodes in the bridge circuitry for multi-level converters are required to prevent conduction via the parasitic FET body diode when the switch is reverse biased while turned off as is the case in some phases of transmission. A second FET connected in series with source and drain reversed can provide the same level of protection when the bridge is switched off. These can either be connected in a source-coupled configuration, or the drain-coupled configuration shown in Figure 1e. This provides an opportunity to push the power handling and speed of the half bridge topology further. When switched on, the additional FETs are required to conduct in reverse. GaN devices are naturally capable of operation in the third quadrant providing high performance reverse conduction [25]. With the diodes removed, the efficiency, speed, and power handling capabilities can be increased due to FETs switching faster and having lower on resistance than diodes. This change

simultaneously produces a full push-pull topology capable of driving complex loads with faithfully produced HRPWM waveforms.

### III. TRANSDUCER POWER OUTPUT MONITORING

#### A. Power Measurement Requirement

Typically, the acoustic output of a system is determined through calibration techniques, using a hydrophone or radiation force balance, where the output of the transducer is measured under specified free-field conditions. Measurement of the transducer bandwidth is typically performed through hydrophone measurements [26], however for HIFU transducers, these are usually taken at lower output powers and the results scaled up to estimate the output at higher powers. This is due to limitations on the power handling capabilities of typical hydrophones, though the use of fibre-optic hydrophones has been proposed to overcome this [27]. To measure the total energy delivered by long duration bursts, calibration measurements are performed using a Radiation Force Balance (RFB) [28].

In addition to calibrating the transducer, the drive system can be calibrated. Measuring the forward and reverse signal voltages delivered into a known load, such as a  $50\ \Omega$  resistor, allows the output levels of the system to be checked and adjusted to produce the expected output across a range of frequencies [6]. However, these approaches do not allow the measurement of the output power during use of the system. Instead, they rely on periodic calibration to ensure that changes to the system over time, such as component ageing, are accounted for. This allows for the possibility of drift in the output power between calibration periods.

Techniques have been presented for the use of power monitoring circuitry measuring the output voltage and current when the system is driving a transducer load in order to calculate the true output power of the system [29], [30], with [29] presenting the argument that electrical output power can be correlated directly to the acoustic power delivered based on the conversion efficiency of the transducer. In both of these examples, the measurement approach was based around the use of an oscilloscope with current and voltage probes in order to measure the power. Real-time monitoring of the output power integrated into the drive system could allow these techniques to be used in practical applications, for not only power monitoring, but also for cavitation detection by monitoring low frequency power fluctuations caused by backscattered signal [31].

Multi-level transmitters generate complex stepped waveforms, as opposed to simple sinusoidal waveforms from typical linear or filtered output transmitters. As such, the calculation of average power cannot be performed using the simplification of half-peak power. Instead, average power measurement is determined by integrating the instantaneous power over time [32]. As the period of the signal is not necessarily an integer factor of the sample rate, the integration is performed by averaging over many cycles ( $> 15$ ) to limit error introduced from sampling a partial waveform period.

When measuring the power output of a HRPWM waveform into a load, only the power delivered at the fundamental, 3rd

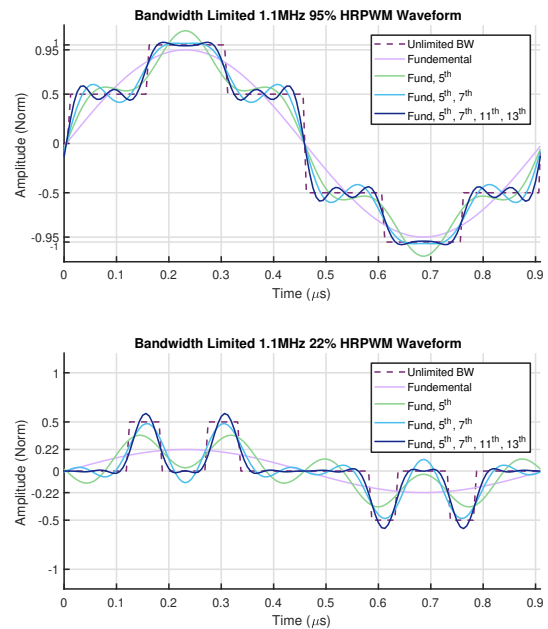


Fig. 2. Harmonic composition of two amplitudes of HRPWM waveforms, showing how the shape of the switched waveforms are formed from a series of odd harmonics. When sampled at rates which exclude high order harmonics as presented in the next section, the measured waveform appear completely different from the excitation sequence in the time domain due to bandwidth limitation.

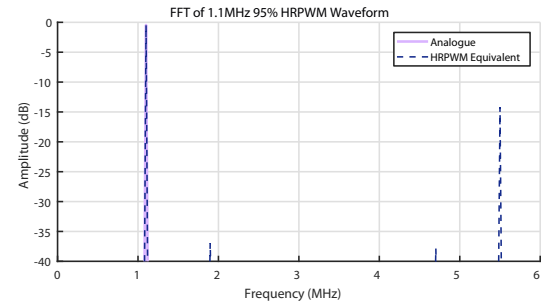


Fig. 3. Spectrum of a 1.1 MHz 95 % HRPWM 40 cycle waveform sampled at  $80\ \text{MS}^{-1}$ , showing spectral artefacts caused the fundamental frequency not being an integer factor of the sample rate.

and, if in-band for the transducer, the 5th, need to be considered. Figure 2 shows the effect of this bandwidth limitation at two different amplitudes of HRPWM, one at 95 %, and the other at 22 %. Furthermore, in Figure 3 the spectrum of the 95 % waveform is shown in the frequency domain for a 1.1 MHz fundamental. The cancellation of the 3rd harmonic in the waveform design is apparent, as are small spurious peaks at non-harmonic locations caused by cycle-to-cycle jitter due to rounding of the transition points to the nearest sample time. The amplitude of these peaks is significantly lower than the fundamental so provide very little contribution in the output waveform.

#### B. Current Measurement Techniques

In order to measure power using integration of instantaneous power, both current and voltage measurements are required. The design of the transmitter for use with array transducers

with a shared ground mandates that the current measurement must be performed using a high-side sensing as all transducer elements share a common return path. High side sensing requires an isolated measurement technique, such as using inductive current transformers and Rogowski coils, using magnetic measurements such as Hall Effect sensors, or using current shunt measurements with additional isolation.

In designing the power measurement circuit, several current measurement techniques were considered. Hall effect sensors though simple to integrate are limited to sub-MHz bandwidths [33], [34] which make them unsuitable for the multi-MHz range required for ultrasound therapy. Current sense transformers are frequently used to perform galvanically isolated current measurements, and are capable of measurements of  $\gg 10$  MHz, however, when such transformers are miniaturized, they suffer from limited bandwidth — for example the CST7030 series by Coilcraft [35], fairly representative of currently available transformers, are limited to sub-MHz. Such transformers can also suffer from core hysteresis and saturation effects at high currents or if DC currents are present [34]. Rogowski coils have also been shown to provide compact high current and frequency capability at frequencies on the order of 1 MHz to 100 MHz with a large current handling capability of  $> 15$  A [36], [37] however were rejected for this design due to the complexity of integration.

Current shunts are the simplest method of measuring current by measuring the voltage drop across a series element. Approaches for shunt measurements come in various forms, from using a series resistor, to using the on-state resistance of MOSFETs in a converter bridge [33], [38]. It is possible to achieve very high bandwidth and accuracy in measurement, especially with resistive shunts, limited only by the acceptable power loss in the shunt element, and the capabilities of the data converters used. However, such shunts do not in themselves provide any form of isolation as is required for high-side sensing. Typical approaches to isolating current shunts are limited either in voltage handling to  $< 50$  V capabilities for direct measurement amplifiers or in terms of bandwidth limitations of  $\ll 500$  kHz for isolated analogue amplifiers.

Modern digital isolator technology can provide high data rate isolation capable of withstanding very high slew rates in excess of  $100 \text{ kV ns}^{-1}$ , whilst also providing an isolated power source [39]. Instead of performing isolation of the analogue signal, a technique of floating an Analogue to Digital Converter (ADC) on the output of the transmitter, and isolating in the digital domain is proposed.

#### IV. HIGH-INTENSITY FOCUSED ULTRASOUND TRANSMITTER WITH INTEGRATED POWER MONITORING

A multi-channel system for HIFU applications developed at the University of Leeds has been previously discussed [9], capable of switching at frequencies up to  $\sim 1.5$  MHz with output powers of up to 50 W. In developing the new high power transmitter presented in this paper, the form factor and electrical connectivity was maintained to allow a direct upgrade of the HIFU Array Research Platform (HIFUARP) system. This form factor set the overall dimensions and

connector positions to a  $10 \times 10$  cm sized module. This size restriction set limits on the complexity of the circuit design, requiring a double-sided 6-layer circuit, which includes the GaN transmitter, power measurement circuitry, and control circuitry. Figure 4 shows a photograph of the manufactured module.

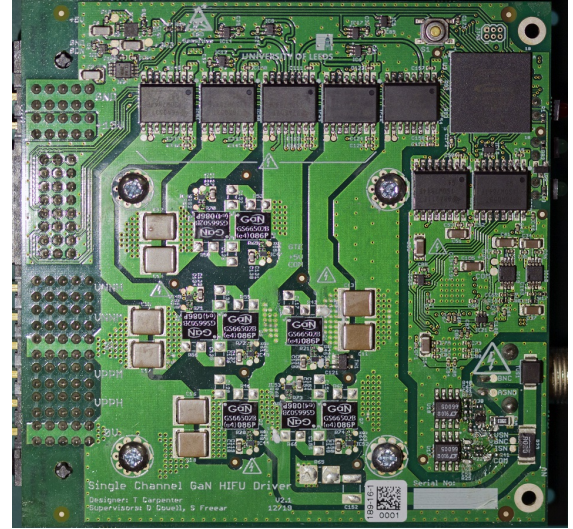


Fig. 4. Photograph of the manufactured and assembled High-Voltage GaN Push-Pull HIFU transmit transmitter with I-V sense circuitry.

##### A. Integrated Power Measurement Circuit

A prototype of the proposed power measurement circuit was previously presented in the form of a conference article [40], which provided a proof of concept method of integrated power measurement circuitry into a HIFU transmitter by performing floating high-side current measurements using an 8 bit  $11 \text{ MS s}^{-1}$  ADC and parallel-to-serial data converter to allow transmission through a low channel count digital isolator. In this work, the design of the prototype has been improved and adapted to allow for an increase in bit depth and higher sampling rate.

In the previous design [40], separate measurement circuits were used for voltage and current measurement, with the voltage measured with a converter referenced to ground. To increase the performance of the measurement circuit without increasing the size of the transmitter, the measurement topology was redesigned to float both the current and voltage measurement on the output, and instead measure the voltage of ground relative to the output, as shown in Figure 5a. Using this measurement topology, it is possible to make use of a single dual-channel ADC whilst simultaneously reducing the amount of components and power supply generation required. The voltage and current measurement blocks can then use identical circuitry, each driving one channel of the data converter. The voltage measurement uses an additional series resistor,  $R_{\text{divider}}$  in Figure 5a, which forms a potential divider with the sense resistor in Figure 5b to attenuate the high output voltage to a safe measurement level.

The ADS6222 (Texas Instruments Inc.) converter was selected as it includes built-in serializers which allow splitting of

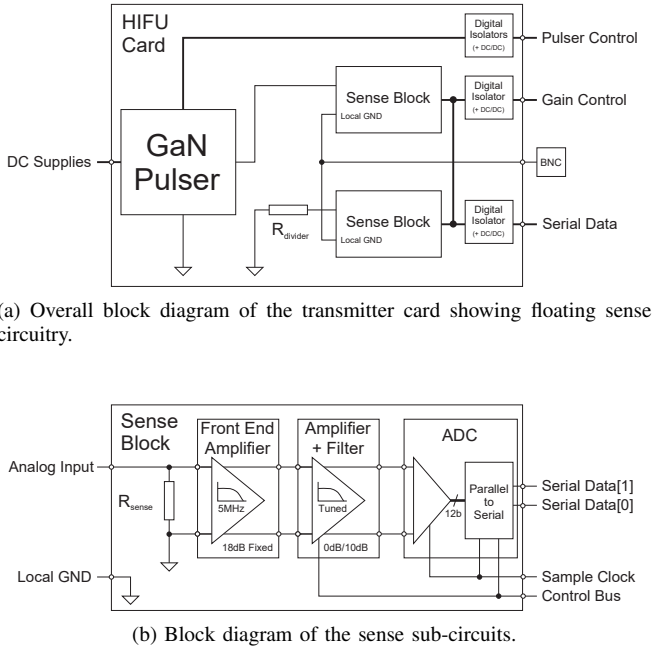


Fig. 5. Block diagram of GaN based HIFUARP card with I-V sense circuitry where both voltage and current measurement floating on the output of the transmitter allowing the use of a dual-channel ADC.

the data stream across two Low-Voltage Differential Signalling (LVDS) pairs at sample rates as low as  $10 \text{ MS s}^{-1}$ . In 12 bit mode using two serial links [41], this allows the sample rate to be increased to  $16 \text{ MS s}^{-1}$  compared with the prototype, as well as increasing the bit depth to 12 bit, by making use of two digital isolator channels per converter channel instead of only one, whilst maintaining a serial data rate below the  $100 \text{ Mbit s}^{-1}$  limit of the ISOW784x series (Texas Instruments Inc.) isolators being used in the design [39].

The measurement sense blocks use an LT6600-5 (Analog Devices) front end amplifier to allow differential measurement of the current shunt. As the voltage measurement uses a very high impedance potential divider to limit power losses, an additional unity gain stable amplifier, is used to buffer the output of the divider, with the ADA4807 (Analog Devices) selected for its very low DC offset [42] rating, and its unity gain stability. Ferrite beads are included in the front end to prevent very high frequency noise from the high-order HRPWM harmonics causing instability in the amplifiers.

The previous design suffered from aliasing issues, with high order harmonics folding back into the Nyquist limited bandwidth of the measurement circuit. A dual channel digitally controllable 6th order low-pass filter and configurable gain amplifier, the HMC900 (Analog Devices), was selected as an additional anti-aliasing filter. When configured as a 4 MHz filter, an attenuation of 40 dB is achieved by the 8 MHz Nyquist frequency [43], in addition to the 12 dB attenuation provided by a filter in the front end amplifier [44]. Ultimately this combination allows for a  $16 \text{ MS s}^{-1}$  12 bit I-V measurement with two selectable gains of 10 dB and 0 dB, along with filtering to remove high-order harmonics from the measurement results. A photograph of the measurement circuit is shown in Figure 6.

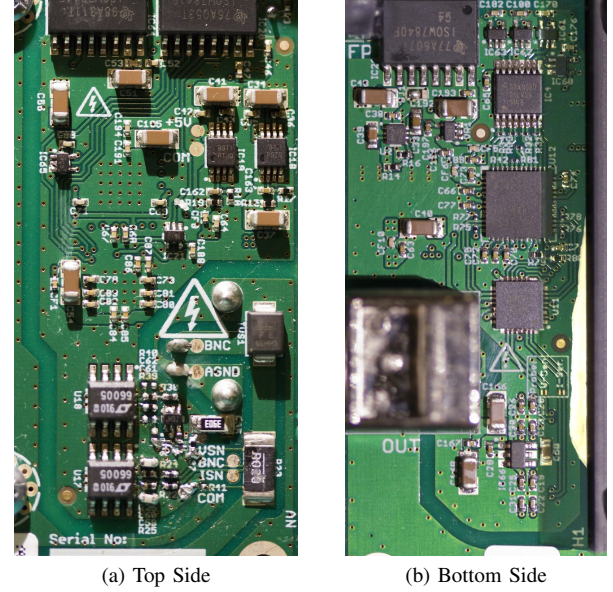


Fig. 6. Photographs of the I-V measurement circuitry on the GaN transmitter card. Front end amplifiers and sense resistors are seen to the bottom of (a). The remaining analogue to digital chain of HMC900 amplifier, ADS6222 ADC, and LVDS to CMOS buffers appear from middle to top in (b).

## B. Gallium-Nitride High-Intensity Focused Ultrasound Transmitter Design

The structure of the transmitter uses the drain coupled half bridge topology proposed in Figure 1e, as the building block for a 5-level transmitter. The transmitter includes drivers for a bipolar outer rail  $+V_{P1}/-V_{N1}$ , a bipolar mid rail  $+V_{P2}/-V_{N2}$ , and a ground clamp circuit GND. The mid-rails,  $+V_{P2}/-V_{N2}$ , use a full bipolar push-pull bridge consisting of four GaN devices, two for each polarity. As the drain coupled structure can conduct in both directions, only one transistor pair is required for the ground clamp circuit. By setting a restriction that the mid voltage rails must be of lower magnitude than the outer rails, it is possible to simplify the outer rail bridge to just two transistors, one to drive to each of  $+V_{P1}$  and  $-V_{N1}$  as these FETs can never be reverse biased. The final bridge structure is shown in 7 [45].

To achieve  $>1 \text{ kW}$  output powers into  $\sim 50 \Omega$  loads, the output waveforms are required to be several hundred volts peak to peak. A high voltage GaN device was selected for this task, the GS66502B (GaN Systems). These devices provide  $<50 \text{ m}\Omega$  on resistance, 650 V drain-source voltage rating, and are capable of switching at over 10 MHz [46]. A total of eight GaN FETs are required, each of which needs an independently isolated control signal. Dedicated GaN gate drivers, LMG1020 (Texas Instruments Inc.), are used to provide high current gate switching, allowing for fast switching whilst allowing for the use of low current digital isolator technology for signal isolation. Ferrite beads were added in series with selected gate drive resistors to prevent oscillation of the transistors and overshoot meaning no snubbing circuits are required on the output.

The drain-coupled structure compared to a source-coupled transistor pair simplifies this control in that four of the

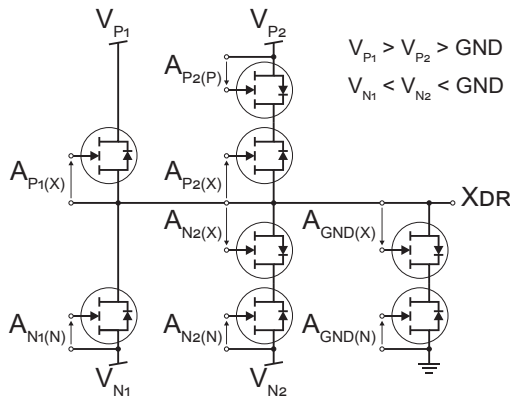


Fig. 7. Full transistor bridge topology for the implemented 5-level push-pull all-GaN transmitter. Digital isolators with integrated isolated DC-DC converters are used to control the FETs with a minimum pulse width on each switch of 10 ns.

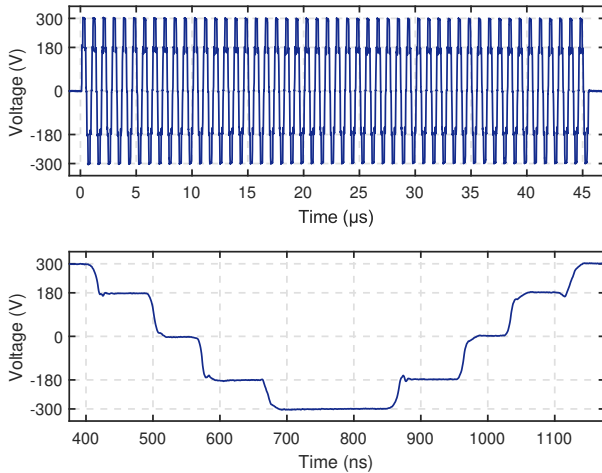


Fig. 8. HIFU transmitter driving a  $50\ \Omega$  load with at 1.1 MHz 5-level HRPWM waveform at its maximum rated output of  $600\ V_{pp}$ , delivering an average power of 225 W (1.8 kW peak) for 45  $\mu$ s.

eight transistors have sources connected to the same voltage reference — the transmitter output — which means they can share the same four channel digital isolator. As the GS66502B devices are bottom-cooled packages, the choice of drain connectivity also aids in cooling of the transistors. The large source pads are all connected to large copper planes for the four power supplies, ground, and output, which aids in transferring heat away from the transistor dies.

In order to allow for flexibility in control, a Max 10 (Intel Corporation) Field Programmable Gate Array (FPGA) was included on the transmitter board. This FPGA was responsible for mapping the original HIFUARP control signals into the necessary FET gate signals, allowing for the control interface to be changed for a next generation Ultrasound Array Research Platform (UARP) system. In addition, the FPGA interfaces with the power monitoring circuit to configure the front end filtering, deserialize and recombine the parallel-serial ADC data streams, and perform power measurement calculations.

## V. EXPERIMENTAL RESULTS

Large single-element HIFU transducers exhibit a wide variety of impedances, though many include tuning circuits to match their impedance to  $\sim 50\ \Omega$  for compatibility with linear amplifiers and a common cabling characteristic impedance. The H-102 transducer used for some measurements in this paper is for example tuned to an impedance of around  $43\ \Omega$  resistive at its fundamental resonant frequency of 1.1 MHz. The use of a matching network is not specifically required for this transmitter as the output impedances is very low ( $< 1\ \Omega$ ). The methodology of this study uses a  $50\ \Omega$  Radio Frequency (RF) load for many of the tests as this provides a safe and consistent method of characterizing the transmitter to a generic load consistent with a matched transducer.

Several tests were performed using the transmitter and measurement circuitry to verify that it can accurately measure the output power of the system, but also to ensure that the transmitter is capable of controlling the output power and operating up to its rated  $600\ V_{pp}$ . Figure 8 shows operation at the full output swing, with the transmitter driving a  $50\ \Omega$  load with a 1.1 MHz 5-level waveform. Due to the available high voltage power supplies, the mid rails were set at  $\pm 180\ V$  rather than the half voltage level ( $\pm 150\ V$ ). Whilst the higher mid-level voltage requires modification of the HRPWM waveform algorithm to achieve harmonic control, it is a limitation of the experimental setup rather than the transmitter itself. The output shows a clean waveform with ringing of less than 10% overshoot, and the output levels showing  $< 1\ V$  drop across the transistors. The waveform also shows the push-pull ability to all levels, with rise/fall times are around 10 ns to slew 180 V.

Temperature measurements were obtained of the transmitter bridge during operation using a thermoIMAGER TIM640 thermal camera (Micro-Epsilon Group). In Figure 9, temperature rise measurements were taken for a 30 s 100% duty-cycle CW  $160\ V_{pp}$  HRPWM waveform driving a  $50\ \Omega$  load, with a thermal image of the transmitter bridge showing the temperature of each of the eight transistors after 30 s, with the ambient temperature of the board measured at  $29\ ^\circ\text{C}$ . Despite being only passively cooled by a natural convection from the heatsink, a temperature rise limited to at most  $32\ ^\circ\text{C}$  above ambient is observed, which is well within the maximum  $150\ ^\circ\text{C}$  junction temperature rating for the devices used. By comparison, the silicon half-bridge design presented in [9] when configured to operate using the same design waveform under the same cooling conditions exhibits a temperature rise of  $51\ ^\circ\text{C}$  to  $82\ ^\circ\text{C}$  as shown in Figure 10. Interestingly, the transistors that provide protection against reverse bias, those which conduct in the reverse direction, show significantly less heating than the other transistors. This shows that the GaN devices are an excellent choice for replacing the reverse protection diodes.

One of the key requirements for the 5-level transmitter is the ability to accurately control the output amplitude using HRPWM waveforms. To determine the amplitude control ability of the transmitter, measurements for multiple different HRPWM amplitudes were obtained for a 1.1 MHz transmission, for both a  $50\ \Omega$  RF load and also an H-102

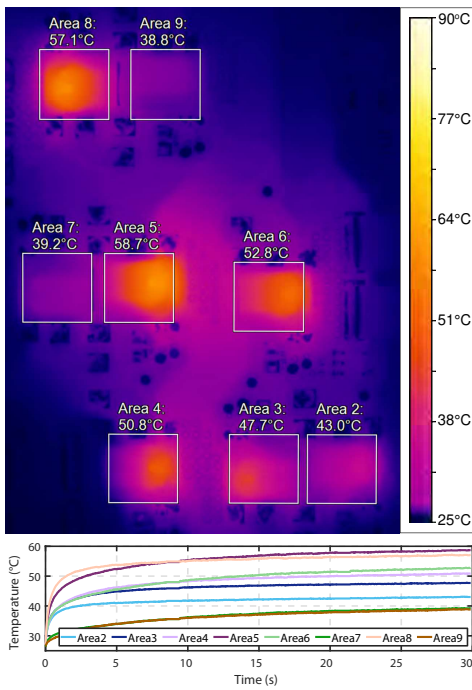


Fig. 9. Thermal image and temperature profiles for new GaN push-pull design, driving a  $50\ \Omega$  load with a 30 s CW at 1.1 MHz  $160\ V_{pp}$  5-level HRPWM waveform. Thermal image shows temperature after 30 s.

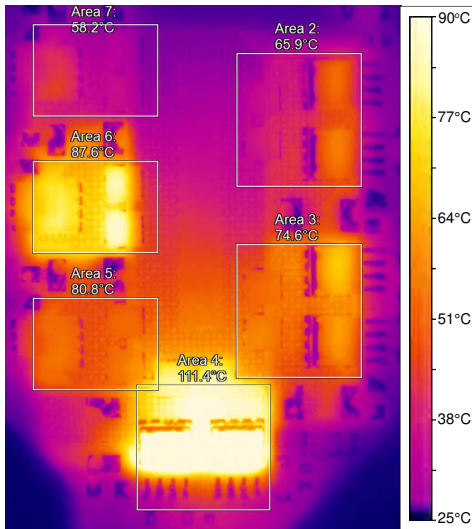


Fig. 10. Comparative thermal image showing temperature after 30 s of previous MOSFET half-bridge design [9] under same drive conditions as Figure 9.

HIFU transducer (Sonic Concepts), for both the new GaN transmitter, and the previous generation silicon half-bridge [9]. The HRPWM amplitude should correspond to the amplitude of the fundamental as a percentage of the outer supply rail,  $V_{s(\text{peak})}$ , which in the case of these tests was set to  $\pm 80\ V$ .

Figure 11 shows a comparison between HRPWM amplitude and output amplitude, for a  $50\ \Omega$  RF load, and a H-102 transducer. The designed waveform is shown in green, the Silicon transmitter in blue, and the GaN transmitter in purple. For each amplitude, (a) shows the output fundamental amplitude, (b) shows the second harmonic amplitude, and (c) shows the

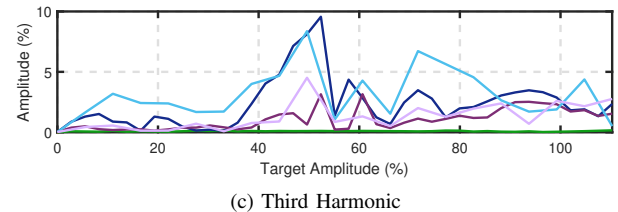
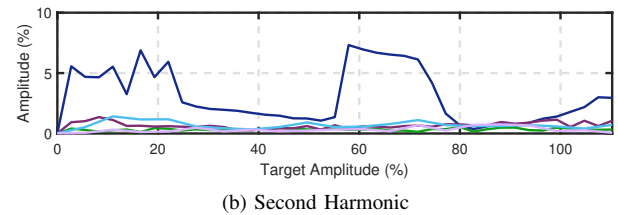
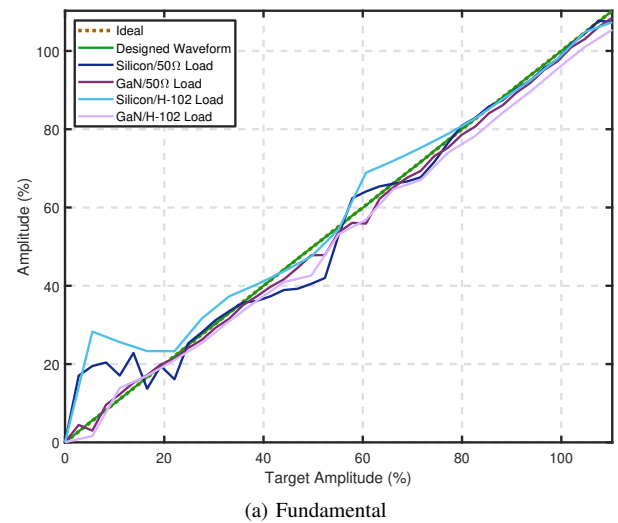


Fig. 11. Measurement of 5-level HRPWM amplitude control performance based in FFT of 1.1 MHz HRPWM electrical output waveforms into a  $50\ \Omega$  and H-102 transducer load, comparing both the silicon transmitter [9] and new GaN transmitter. Amplitudes are normalized to  $160\ V_{pp}$ .

third harmonic amplitude, as calculated from the measured output voltage waveform from the transmitters. It can be seen that the new transmitter design with its faster switching ability is capable of providing an improved ability to generate the designed HRPWM waveforms, particularly at the mid-range and low-range amplitudes where narrow pulses ( $< 20\ \text{ns}$ ) are required. The ability to switch at higher frequencies also allows for improved third harmonic control, whilst the push-pull and symmetric design removes the majority of the second harmonic distortion.

Figure 12 shows a series of time domain and frequency domain plots of voltage and current measurements for 22% and 95% amplitudes at a 1.1 MHz fundamental frequency along with 95% amplitude measurements at 3.3 MHz frequency, for a  $50\ \Omega$  RF load. Additionally, power measurements for a 1.1 MHz waveform driving an H-102 Transducer (Sonic Concepts) are shown. In each case the power is measured as the average over a  $300\ \mu\text{s}$  interval. Reference current and voltage measurements using an MSO-S 204A oscilloscope

(Keysight Technologies) coupled with an N2873A passive voltage probe (Keysight Technologies) and N2893A active current probe (Keysight Technologies) are shown in purple, and measurements using the integrated I-V circuit are shown in blue.

For the 22% amplitude, the time domain waveform, Figure 12a, appears to overshoot and undershoot compared to the oscilloscope waveform, however as was shown in Figure 2, this is fully expected for a bandwidth limited HRPWM signal measurement for this amplitude. In fact comparing the frequency domain, Figure 12b, the results show similar amplitude peaks in the same locations for both oscilloscope and I-V, for both voltage and current. The spurious peaks at 1.9 MHz and 4.7 MHz are caused by the fundamental frequency being a non-integer factor of the transmission sample rate.

In each of the measurements the spectrum is significantly cleaner than that of the original work presented work [40] due to the improved analogue front end design, higher sampling rate, and improved anti-aliasing filtering. The peaks in the frequency domain are also significantly sharper than in the previous design. This suggests that the sampling clock for the ADC has a sufficiently low jitter, which helps to avoid excessive phase noise. Furthermore, the power measurements at 1.1 MHz for both the resistive load and complex transducer load, shows differences of less than 2 W from the corresponding oscilloscope measurements compared with typically 6 W differences for the previous front end design. In the case of Figure 12f, the current measurements contain a number of non-harmonic spikes in the 2 MHz to 3 MHz range, in both the oscilloscope and sense circuit measurements, which are caused the complex behaviour of the transducer when driven by a stepped waveform. Such spectral content is also present if the transducer is driven with a stepped waveform using an A150 300 kHz to 35 MHz linear power amplifier (E&I Ltd.) and 33612A signal generator (Keysight Technologies), and therefore are not caused specifically by the design of the transmitter.

Power measurements can also be performed at higher frequencies, with measurements shown in Figure 12g and 12h for a 3.3 MHz output. At this frequency only the fundamental can be measured due to the limited Nyquist measurement bandwidth. Despite this, the floating analogue front end is able to perform accurate measurements of the output power, with the measurement circuit reading with 2% of the reference oscilloscope power measurement.

## VI. CONCLUSIONS

In this study, a high power ultrasound transmitter with real time power monitoring has been demonstrated for HIFU applications. The transmitter is capable of handling both very high power, 1.8 kW peak powers using 600 V<sub>pp</sub> for short burst applications (<20 ms), and providing sustained CW transmit powers of >140 W for >30 s at typical frequencies used for HIFU therapy.

The previous generation Silicon half-bridge design presented in [9] was limited in performance the range of 0 MHz to 1.5 MHz and suffered from large second harmonic distortion

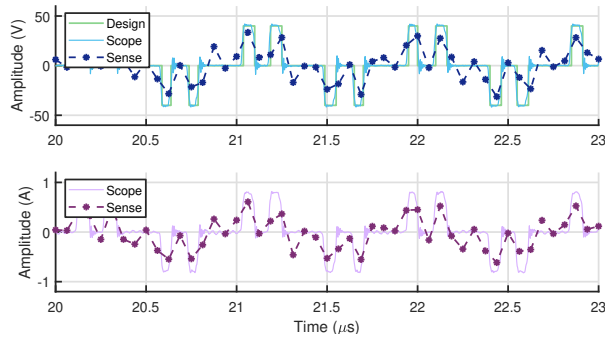
and poor amplitude control as a result of limited switching performance. The 5-level push-pull structure in the presented design allows for faithful HRPWM generation with minimal dead-time requirements. This ensures accurate amplitude control of the output signal, minimal second harmonic generation, and a large reduction in the power of the third harmonic in the drive waveform. As there is no output transformer or filtering required, and the output is low impedance, the transmitter is capable of working over a very wide range of frequencies from DC (0 Hz) through to 5 MHz, whilst allowing for very high power outputs into unmatched loads.

I-V measurement circuitry integrated into the transmitter has been demonstrated as capable of measuring the true real power delivered to even complex loads. This power measurement is capable of accurately measuring the delivered power into both resistive and transducer loads, allowing for calibration of the electrical output power of the system to maintain safe exposure levels, and to protect the transducer. By using an isolated high-side measurement circuit, it is possible to use the design in conjunction with multi-element transducers with a common ground. The compact size of the drive circuitry is further conducive to scaling for multi-element transducers.

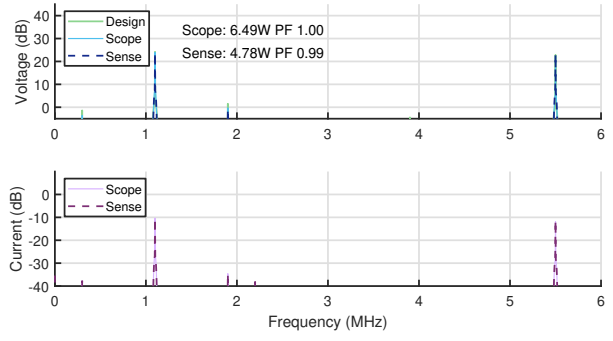
The transmitter implementation has been designed for integration into the University of Leeds mixed-modality UARP systems to allow for direct combination with ultrasound imaging mobilities to perform ultrasound guided HIFU therapy. The architecture has been demonstrated to offer superior performance compared to the previous generation Silicon half-bridge design, with improved harmonic control and power handling.

## REFERENCES

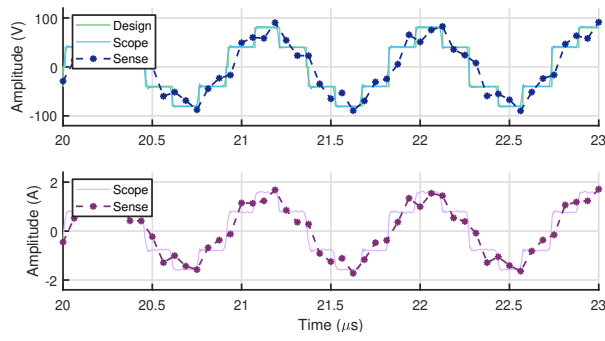
- [1] G. T. Haar, "Ultrasound focal beam surgery," *Ultrasound in Medicine & Biology*, vol. 21, no. 9, pp. 1089–1100, Jan. 1995.
- [2] M. Lee, D. Schlesinger, G. ter Haar, B. Sela, M. Eames, J. Snell, A. Hananel, N. Kassell, J. Sheehan, J. Larner, and J.-F. Aubry, "Thermal dose and radiation dose comparison based on cell survival," *Journal of Therapeutic Ultrasound*, vol. 3, no. S1, Jun. 2015.
- [3] V. A. Khokhlova, M. R. Bailey, J. A. Reed, B. W. Cunitz, P. J. Kaczowski, and L. A. Crum, "Effects of nonlinear propagation, cavitation, and boiling in lesion formation by high intensity focused ultrasound in a gel phantom," *The Journal of the Acoustical Society of America*, vol. 119, no. 3, pp. 1834–1848, Mar. 2006.
- [4] J. R. McLaughlan, D. M. J. Cowell, and S. Freear, "Gold nanoparticle nucleated cavitation for enhanced high intensity focused ultrasound therapy," *Physics in Medicine & Biology*, vol. 63, no. 1, p. 015004, Dec. 2017.
- [5] Z. Izadifar, P. Babyn, and D. Chapman, "Mechanical and Biological Effects of Ultrasound: A Review of Present Knowledge," *Ultrasound in Medicine & Biology*, vol. 43, no. 6, pp. 1085–1104, Jun. 2017.
- [6] M. M. El-Desouki and K. Hynynen, "Driving Circuitry for Focused Ultrasound Noninvasive Surgery and Drug Delivery Applications," *Sensors*, vol. 11, no. 1, pp. 539–556, Jan. 2011.
- [7] K. D. Evans, B. Weiss, and M. Knopp, "High-Intensity Focused Ultrasound (HIFU) for Specific Therapeutic Treatments: A Literature Review," *Journal of Diagnostic Medical Sonography*, vol. 23, no. 6, pp. 319–327, Nov. 2007.
- [8] G. Fleury, "Safety Issues for HIFU Transducer Design," in *AIP Conference Proceedings*, vol. 754, no. 1. AIP, 2005, pp. 233–241.
- [9] C. Adams, T. M. Carpenter, D. Cowell, S. Freear, and J. R. McLaughlan, "HIFU Drive System Miniaturization Using Harmonic Reduced Pulse Width Modulation," *IEEE Transactions on Ultrasonics, Ferroelectrics, and Frequency Control*, vol. 65, no. 12, pp. 2407–2417, Dec. 2018.



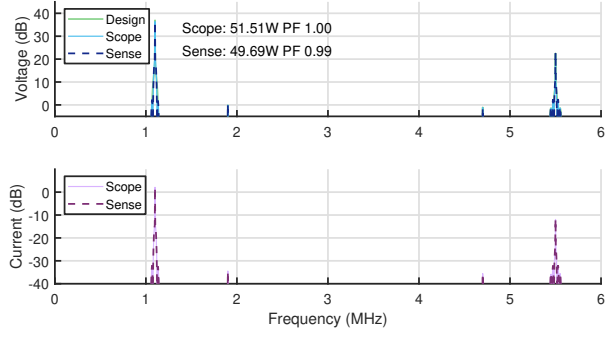
(a) Time Domain — 1.1 MHz 22% Amplitude, 50  $\Omega$  Load



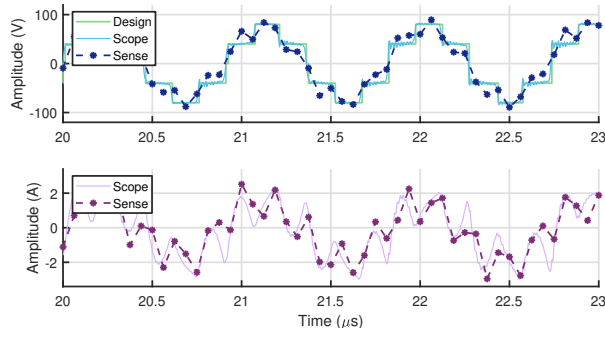
(b) Frequency Domain — 1.1 MHz 22% Amplitude, 50  $\Omega$  Load



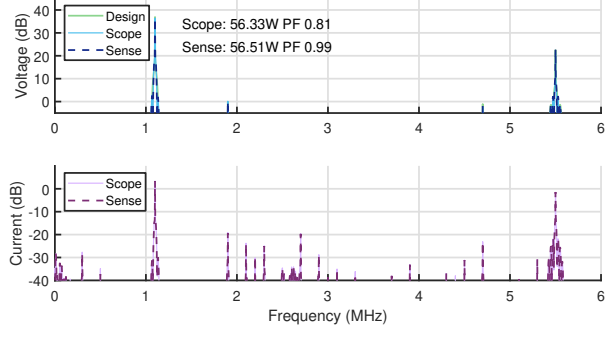
(c) Time Domain — 1.1 MHz 95% Amplitude, 50  $\Omega$  Load



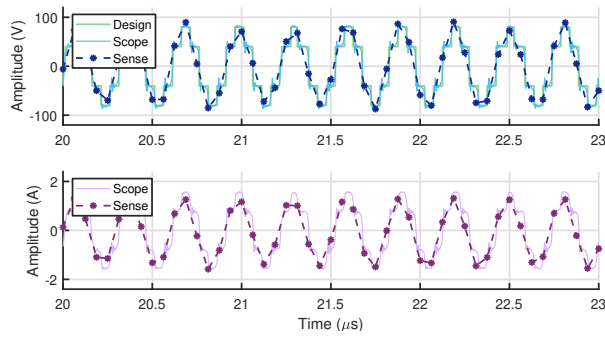
(d) Frequency Domain — 1.1 MHz 95% Amplitude, 50  $\Omega$  Load



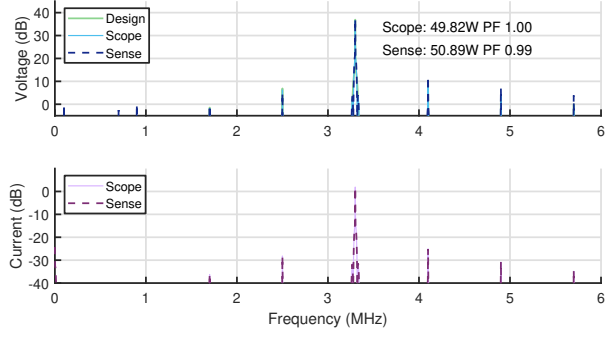
(e) Time Domain — 1.1 MHz 95% Amplitude, H-102 Transducer



(f) Frequency Domain — 1.1 MHz 95% Amplitude, H-102 Transducer



(g) Time Domain — 3.3 MHz 95% Amplitude, 50  $\Omega$  Load



(h) Frequency Domain — 3.3 MHz 95% Amplitude, 50  $\Omega$  Load

Fig. 12. Current and Voltage measurements acquired using an MSO-S 204A oscilloscope (Keysight Technologies) vs those acquired using the presented integrated I-V sense circuitry. In each case drive rails of  $\pm 80$  V,  $\pm 40$  V, along with ground were used to produce amplitude controlled HRPWM waveforms using the GaN transmitter bridge. Two loads were tested, a 50  $\Omega$  RF load, and a H-102 HIFU transducer (Sonic Concepts) as indicated in the figure captions.

- [10] C. Christoffersen, W. Wong, S. Pichardo, G. Togtema, and L. Curiel, "Class-DE Ultrasound Transducer Driver for HIFU Therapy," *IEEE Transactions on Biomedical Circuits and Systems*, vol. 10, no. 2, pp. 375–382, Apr. 2016.
- [11] R. Seip, W. Chen, J. Tavakkoli, L. A. Frizzell, and N. T. Sanghvi, "High-intensity focused ultrasound (HIFU) phased arrays: Recent developments in transrectal transducers and driving electronics design," in *Proc. 3rd Int. Symp. Therapeutic Ultrasound*, 2003, pp. 423–428.
- [12] S. C. Tang and G. T. Clement, "A harmonic cancellation technique for an ultrasound transducer excited by a switched-mode power converter," in *2008 IEEE Ultrasonics Symposium*. IEEE, Nov. 2008, pp. 2076–2079.
- [13] Sonic Concepts, "H-Transducer Series 64 mm Datasheet," 2018, Accessed: 2018. [Online]. Available: [http://sonicconcepts.com/wp-content/uploads/2016/05/H-%C3%BF64\\_DataSheet\\_B.pdf](http://sonicconcepts.com/wp-content/uploads/2016/05/H-%C3%BF64_DataSheet_B.pdf)
- [14] Precision Acoustics, "HIFU Transducers Datasheet," 2018, Accessed: 2018. [Online]. Available: <https://www.acoustics.co.uk/product/hifu-transducers/>
- [15] Q. Stedman, L. Gu, C.-N. Pai, M. Rasmussen, K. Brenner, B. Ma, A. S. Ergun, J. R. Davila, and B. Khuri-Yakub, "Compact Fast-Switching DC and Resonant RF Drivers for a Dual-Mode Imaging and HIFU 2D CMUT Array," in *2019 IEEE International Ultrasonics Symposium (IUS)*. IEEE, Oct. 2019.
- [16] P. R. Smith, D. M. J. Cowell, and S. Freear, "Width-modulated square-wave pulses for ultrasound applications," *IEEE Transactions on Ultrasonics, Ferroelectrics, and Frequency Control*, vol. 60, no. 11, pp. 2244–2256, Nov. 2013.
- [17] D. M. J. Cowell, T. Carpenter, P. Smith, C. Adams, S. Harput, and S. Freear, "Performance of switched mode arbitrary excitation using Harmonic Reduction Pulse Width Modulation (HRPWM) in array imaging applications," in *2016 IEEE International Ultrasonics Symposium (IUS)*. IEEE, Sep. 2016.
- [18] S. Freear, D. M. J. Cowell, and P. R. Smith, "Ultrasound Generation," United Kingdom patent WO2014096789A2, 2014.
- [19] Maxim Integrated, "Octal Three-Level/Quad Five-Level High-Voltage 2A Digital Pulsers with T/R Switch," MAX14808 Datasheet, Jan. 2014.
- [20] L. Svilainis, A. Chaziachmetovas, and V. Dumbrava, "Half bridge topology 500V pulser for ultrasonic transducer excitation," *Ultrasonics*, vol. 59, pp. 79–85, May 2015.
- [21] D. M. J. Cowell, C. Adams, T. M. Carpenter, and S. Freear, "Modified Harmonic Reduction Pulse Width Modulation (mHRPWM) for Switched Excitation of Resonant HIFU Transducers," in *2018 IEEE International Ultrasonics Symposium (IUS)*, Oct. 2018, pp. 1–4.
- [22] L. Svilainis, V. Dumbrava, and A. Chaziachmetovas, "Investigation of the Half Bridge and Transformer Push-Pull Pulser Topologies for Ultrasonic Transducer Excitation," *Journal of Circuits, Systems and Computers*, vol. 24, no. 05, p. 1550062, Aug. 2015.
- [23] A. Chaziachmetovas, T. E. G. Alvarez-Arenas, and L. Svilainis, "Comparison of Direct and Transformer Drive High Voltage Ultrasonic Pulser Topologies," in *2017 9th IEEE International Conference on Intelligent Data Acquisition and Advanced Computing Systems: Technology and Applications (IDAACS)*, vol. 2. IEEE, Sep. 2017, pp. 1111–1116.
- [24] H. Peng, J. Sabate, K. A. Wall, and J. S. Glaser, "GaN-Based High-Frequency High-Energy Delivery Transformer Push-Pull Inverter for Ultrasound Pulsing Application," *IEEE Transactions on Power Electronics*, vol. 33, no. 8, pp. 6794–6806, Aug. 2018.
- [25] GaN Systems, "Design with GaN Enhancement mode HEMT," GaN Systems Inc., App. Note GN001, Oct. 2016. [Online]. Available: [https://gansystems.com/wp-content/uploads/2018/01/GN001\\_GaNSystems\\_Design\\_with\\_GaN\\_EHEMT\\_Rev3\\_20161007.pdf](https://gansystems.com/wp-content/uploads/2018/01/GN001_GaNSystems_Design_with_GaN_EHEMT_Rev3_20161007.pdf)
- [26] Y. Liu, K. A. Wear, and G. R. Harris, "Variation of High-Intensity Therapeutic Ultrasound (HITU) Pressure Field Characterization: Effects of Hydrophone Choice, Nonlinearity, Spatial Averaging and Complex Deconvolution," *Ultrasound in Medicine & Biology*, vol. 43, no. 10, pp. 2329–2342, Oct. 2017.
- [27] Y. Zhou, L. Zhai, R. Simmons, and P. Zhong, "Measurement of high intensity focused ultrasound fields by a fiber optic probe hydrophone," *The Journal of the Acoustical Society of America*, vol. 120, no. 2, pp. 676–685, Aug. 2006.
- [28] IEC, "Ultrasonics-Field characterization-Specification and measurement of field parameters for high intensity therapeutic ultrasound (HITU) transducers and systems," International Electrotechnical Commission, Standard IEC TS 62556:2014, Apr. 2014.
- [29] B. Karaböce, Y. Gülmez, S. Rajagapol, and A. Shaw, "Instantaneous input electrical power measurements of HITU transducer," *Journal of Physics: Conference Series*, vol. 279, p. 012011, Feb. 2011.
- [30] C. Adams, J. R. McLaughlan, T. M. Carpenter, and S. Freear, "HIFU Power Monitoring Using Combined Instantaneous Current and Voltage Measurement," *IEEE Transactions on Ultrasonics, Ferroelectrics, and Frequency Control*, vol. 67, no. 2, pp. 239–247, Feb. 2020.
- [31] J. McLaughlan, I. Rivens, T. Leighton, and G. ter Haar, "A Study of Bubble Activity Generated in Ex Vivo Tissue by High Intensity Focused Ultrasound," *Ultrasound in Medicine & Biology*, vol. 36, no. 8, pp. 1327–1344, Aug. 2010.
- [32] L. T. Coffeen and J. E. McBride, "High voltage AC resistive current measurements using a computer based digital watts technique," *IEEE Transactions on Power Delivery*, vol. 6, no. 2, pp. 550–556, Apr. 1991.
- [33] M. Biglarbegian, S. J. Nibir, H. Jafarian, and B. Parkhideh, "Development of current measurement techniques for high frequency power converters," in *2016 IEEE International Telecommunications Energy Conference (INTELEC)*. IEEE, Oct. 2016.
- [34] C. Xiao, L. Zhao, T. Asada, W. G. Odendaal, and J. D. van Wyk, "An overview of integratable current sensor technologies," in *38th IAS Annual Meeting on Conference Record of the Industry Applications Conference, 2003*. IEEE, 2003.
- [35] Coilcraft, "CST7030 Series SMT Current Sense Transformers," 2015.
- [36] L. Dalessandro, N. Karrer, and J. W. Kolar, "High-Performance Planar Isolated Current Sensor for Power Electronics Applications," *IEEE Transactions on Power Electronics*, vol. 22, no. 5, pp. 1682–1692, Sep. 2007.
- [37] Y. Xue, J. Lu, Z. Wang, L. M. Tolbert, B. J. Blalock, and F. Wang, "A compact planar Rogowski coil current sensor for active current balancing of parallel-connected Silicon Carbide MOSFETs," in *2014 IEEE Energy Conversion Congress and Exposition (ECCE)*. IEEE, Sep. 2014.
- [38] A. Patel and M. Ferdowsi, "Current Sensing for Automotive Electronics—A Survey," *IEEE Transactions on Vehicular Technology*, vol. 58, no. 8, pp. 4108–4119, Oct. 2009.
- [39] Texas Instruments, "ISOW784x High-performance, 5000-VRMS reinforced quad-channel digital isolators with integrated high-efficiency, low-emissions DC-DC converter," [ISOW784x Datasheet], Mar. 2017, [Revised March 2019]. [Online]. Available: <http://www.ti.com/lit/ds/symlink/isow7840.pdf>
- [40] T. M. Carpenter, D. M. J. Cowell, H. R. Clegg, J. McLaughlan, and S. Freear, "Gallium Nitride Based High-Power Switched HIFU Pulser with Real-Time Current/Voltage Monitoring," in *2019 IEEE International Ultrasonics Symposium (IUS)*, Oct. 2019, pp. 1–4.
- [41] Texas Instruments, "Dual Channel, 12-Bit, 125/105/80/65MSPS ADC With Serial LVDS Interface," ADS6222 Datasheet, May 2007, [Revised January 2014]. [Online]. Available: <https://www.ti.com/lit/gpn/ads6222>
- [42] Analog Devices, "3.1 nV/√Hz, 1 mA, 180 MHz, Rail-to-Rail Input/Output Amplifiers," ADA4807 Datasheet, 2014, [Revision B]. [Online]. Available: [https://www.analog.com/media/en/technical-documentation/data-sheets/ADA4807-1\\_4807-2\\_4807-4.pdf](https://www.analog.com/media/en/technical-documentation/data-sheets/ADA4807-1_4807-2_4807-4.pdf)
- [43] —, "50 MHz Dual Programmable Low Pass Filter With Driver," HMC900 Datasheet, 2013, [Accessed 2020]. [Online]. Available: <https://www.analog.com/media/en/technical-documentation/data-sheets/hmc900.pdf>
- [44] —, "Very Low Noise, Differential Amplifier and 5MHz Lowpass Filter," LT6600-5 Datasheet, 2004. [Online]. Available: <https://www.analog.com/media/en/technical-documentation/data-sheets/66005fb.pdf>
- [45] T. M. Carpenter, D. M. J. Cowell, and S. Freear, "Ultrasound Transmitter," UK Patent Application. Patent Application Number 2019565.7, Dec., 2020, patent applied for.
- [46] GaN Systems, "Bottom-side Cooled 650 V E-Mode GaN Transistor Datasheet," [GS66502B Datasheet], Apr. 2018, [Revised April 2020]. [Online]. Available: <https://gansystems.com/wp-content/uploads/2020/04/GS66502B-DS-Rev-200402.pdf>



**Thomas M. Carpenter (IEEE S'19)** received the M.Eng. degree in electronic and electrical engineering from the University of Leeds, Leeds, UK, in 2014. From 2014 through 2016 he was a Research Engineer at Georgia Institute of Technology, Atlanta, GA, USA, developing high-speed FPGA designs for ultrasound imaging applications. He is currently a Research Assistant with the Ultrasound Research Group at the University of Leeds, developing technology for ultrasound instrumentation systems, and in 2021 completed his PhD studies. His current

research interests include FPGA technology, Embedded Systems, and High-Speed Circuit Design for biomedical and industrial applications.



**David Cowell** received his PhD at the University of Leeds in 2008 for research on advanced coding techniques and excitation circuit design for ultrasonic industrial measurement and medical imaging systems. During this time, he performed extensive consultancy in instrumentation, FPGAs, and high-speed digital hardware design. Following work as a research consultant in measurement and instrumentation, he joined the Ultrasound Group in Leeds as a Research Fellow where his research is currently focused on non-invasive industrial ultrasound measurement and also covers advanced miniaturized ultrasound excitation systems with low harmonic distortion for phased array imaging, ultrasound system design, and signal processing.

measurement and also covers advanced miniaturized ultrasound excitation systems with low harmonic distortion for phased array imaging, ultrasound system design, and signal processing.



**Steven Freear (IEEE S'95–M'97–SM'11)** earned his doctorate in 1997 and subsequently worked in the medical industry for seven years as an electronic system designer. He was appointed Assistant Professor, Associate Professor and then Professor with the School of Electronic and Electrical Engineering at the University of Leeds, Leeds, UK., in 2006, 2008 and 2016, respectively. In 2006, he formed the Ultrasound and Embedded Systems Group, specializing in both industrial and biomedical research. His main research interest is concerned with advanced

analogue and digital signal processing and efficient embedded systems design. He teaches digital signal processing, VLSI and embedded systems design, and hardware description languages at both undergraduate and postgraduate levels. He is Vice President for Publications for the IEEE Ultrasonics, Ferroelectrics and Frequency Control Society (UFFC) having previously served as Editor-in-Chief of the Transactions on UFFC (2013-2018). He was Visiting Professor at Georgia Tech from 2014-2018 where he led development of the imaging engine for an MRI compatible CMUT intravascular catheter funded by NIH/Siemens.



**Harry R. Clegg (IEEE S'19)** received his Electronic Engineering M.Eng. degree from the University of Leeds in 2018. He is currently pursuing a PhD with the Ultrasound and Instrumentation Group in the School of Electronic and Electrical Engineering. His research currently involves the use of Graphics Processing Units (GPUs) and Field-Programmable Gate Arrays (FPGAs) for centralised and distributed beamforming algorithms (turning raw digital data into images in real-time), as well as techniques for enabling simultaneous multi-mode research (where

both ultrasound images for diagnostics and high-energy ultrasound for therapy are used at the same time).



**James R. McLaughlan** received his M.Phys. degree from the physics department at Bath University, where he spent a year working with high power lasers at the Rutherford Appleton Laboratories in Oxfordshire. He completed his Ph.D. at the Institute of Cancer Research (University of London), investigating the optimisation of high intensity focused ultrasound (HIFU) cancer treatments through the use of cavitation. After this, he started as a postdoctoral research assistant in the Mechanical Engineering department at Boston University (USA), where he

investigated the use of light absorbing nanoparticles for cancer imaging and therapy. He joined the ultrasound and instrumentation research group in the School of Electronic and Electrical Engineering at the University of Leeds in 2010, where he was working as part of multidisciplinary team engineering therapeutic microbubbles for the treatment of colorectal cancer. This work is currently undergoing pre-clinical testing with an aim towards 'first in man' studies. In 2013, he was awarded a Leverhulme early career fellowship for a project entitled 'Nanobombs for breast cancer diagnosis and therapy', where he is combining cancer targeted nanoparticles with light and sound for a novel approach for the identification and treatment of early breast cancer. Midway through 2018 he was awarded a UKRI innovation fellowship to develop the use of HIFU with nanoparticles in the treatment of Head and Neck cancers. Currently, he is an associate professor working between the faculties of Engineering and Medicine and Health, where his broad aims are to develop minimally invasive technologies for cancer imaging and therapy for both pre-clinical and clinical applications.